Original Article

Check for updates

Available online at
www.heca-analitika.com/ijds

Infolitika Journal of Data Science

Vol. 3, No. 2, 2025

Comparison of Spatial Interpolation Methods: Inverse Distance Weighted and Kriging for Earthquake Intensity Mapping in Aceh, Indonesia

Latifah Rahayu [1], Cut Chairilla Yolanda Utami [1], Rahmatul Fauzi [1] and Novi Reandy Sasmita [1,*]

[1] Department of Statistics, Faculty of Mathematics and Natural Sciences, Universitas Syiah Kuala, Banda Aceh 23111, Indonesia; latifah.rahayu@usk.ac.id (L.R.); chairilla@mhs.usk.ac.id (C.C.Y.U.); rahmatulfz@mhs.usk.ac.id (R.F.); novireandys@usk.ac.id (N.R.S.)

* Correspondence: novireandys@usk.ac.id

Article History

Received 16 September 2025
Revised 14 November 2025
Accepted 19 November 2025
Available Online 28 November 2025

Keywords:
Spatial interpolation
Kriging
Inverse Distance Weighted (IDW)
Earthquake intensity mapping
Geostatistical analysis

Abstract

Aceh Province, located in the Sumatra megathrust zone of Indonesia, is one of the most seismically active regions in Southeast Asia. Understanding the spatial distribution of earthquake magnitudes is essential for disaster mitigation and risk management. This study compares two spatial interpolation methods Inverse Distance Weighted (IDW) and Kriging to determine the most accurate approach for mapping earthquake intensity in Aceh Province. A total of 2,255 earthquake events with magnitudes of 2.5 M and above, recorded between 1990 and 2024 by the United States Geological Survey (USGS), were analyzed. IDW was tested using five power parameters (p = 1–5), while Kriging applied three semivariogram models (spherical, exponential, and Gaussian). The interpolation accuracy was assessed through Root Mean Square Error (RMSE), Mean Square Error (MSE), and Mean Absolute Percentage Error (MAPE). Results indicated that Kriging with the exponential semivariogram achieved the highest accuracy, with RMSE = 0.0848, MSE = 0.0072, and MAPE = 1.14%, outperforming IDW (RMSE = 0.2288, MSE = 0.0523, MAPE = 1.24%). The Kriging model effectively represented the gradual spatial decay of seismic energy, identifying Aceh Singkil and northern Simeulue as the most earthquake-prone zones, consistent with regional tectonic patterns. These findings confirm that incorporating spatial autocorrelation enhances interpolation accuracy and geophysical interpretation. The study establishes Kriging as a reliable tool for seismic hazard mapping and provides valuable insights for disaster preparedness, infrastructure planning, and future geostatistical applications in earthquake risk assessment.

1. Introduction

Aceh Province, located at the northern tip of Sumatra, lies directly above the Sunda megathrust where the Indo-Australian plate subducts beneath the Eurasian and Burma plates, making it one of the most seismically active regions on Earth [1]. The 26 December 2004 Sumatra–Andaman megathrust earthquake (Mw 9.1–9.3) ruptured a very long segment of this plate boundary and generated the catastrophic Indian Ocean tsunami, causing more than 170,000 fatalities in Aceh alone and over 230,000 deaths across 14 countries [2–4]. This disaster fundamentally changed local and national perspectives on seismic and tsunami risk, prompting substantial investments in early warning systems, reconstruction, and disaster preparedness. In such a tectonically complex setting with a history of megathrust earthquakes and evidence for multi-century recurrence of great events along the Aceh–Andaman segment, reliable spatial information on earthquake hazard is crucial for land use planning, infrastructure design, and disaster risk reduction [5].

In recent decades, dense instrumental earthquake catalogues such as those curated by the U.S. Geological Survey (USGS) have become key resources for quantitative seismic hazard assessment, providing hypocenters and magnitudes over multi-decadal periods [6]. In Indonesia, several studies have used such data to construct local or regional hazard maps. For example, Mase et al. developed response-spectra-based seismic hazard maps for Bengkulu City, highlighting spatial variations in ground-motion levels that are relevant for building codes and engineering design [7]. More recently, robust Ordinary Kriging was applied to map the spatial distribution of earthquake magnitudes in Bengkulu Province, revealing clusters of higher-magnitude events and demonstrating the usefulness of geostatistical interpolation for identifying high-risk areas [8]. In Java, spatial analysis of earthquake intensity distribution has shown that geospatial techniques can enhance understanding of seismic patterns but also noted that comprehensive interpolation analyses remain relatively scarce in Indonesian earthquake research [9]. Beyond seismology, geostatistical methods such as Kriging have been used in Indonesia for environmental and ecological applications, including mangrove site-suitability mapping, underscoring their versatility for spatial decision support [10].

Spatial interpolation plays a central role in these applications by transforming discrete earthquake observations into continuous surfaces representing intensity or magnitude fields. Among the many available interpolation techniques, Inverse Distance Weighting (IDW) and Kriging are two of the most widely used. IDW is a deterministic method that assigns weights to observations based solely on distance, with closer points exerting stronger influence on the estimate; its simplicity and ease of implementation have made it popular in operational mapping [11]. Kriging, in contrast, is a geostatistical estimator that combines distance with a model of spatial autocorrelation derived from the semivariogram, and it can provide both predictions and associated uncertainty [12–14]. Comparative studies in various domains ranging from structural lineament extraction from digital elevation models [15], soil organic carbon stock estimation [16], to climate variable interpolation across complex terrain [17], generally report that Kriging yields lower prediction errors than IDW when the underlying process exhibits moderate to strong spatial dependence. However, results are context-dependent: performance differences can be small in some settings, and the extent to which these findings transfer to highly clustered, fault-controlled seismicity is not always clear.

Despite the growth of geostatistical applications in Indonesian geoscience, there remains a specific gap concerning the performance of IDW versus Kriging for earthquake magnitude mapping in Aceh. Existing Indonesian studies on seismic hazard either focus on different regions (e.g., Bengkulu, Java) [7], or adopt a single interpolation family often Kriging without systematically benchmarking it against IDW using a long-term earthquake catalogue [8]. Moreover, most comparative studies between IDW and Kriging have been conducted for environmental variables rather than seismic data [18]. The spatial distribution of earthquake magnitudes in Aceh is strongly influenced by megathrust segments, the Great Sumatran Fault, and offshore fault systems, leading to anisotropic patterns and potential non-stationarity in the mean field. These characteristics raise methodological questions about which interpolation strategy provides the most reliable representation of historical seismicity, and how model choice might affect the delineation of zones deemed “high risk” by planners and emergency managers. Misclassification of such zones could have tangible consequences for settlement expansion, infrastructure placement, and prioritization of mitigation investments.

Accordingly, the primary research problem addressed in this study is to identify which of two widely used interpolation methods (IDW and Kriging) provides the most accurate and geophysically meaningful representation of the spatial distribution of earthquake magnitudes in Aceh based on a multi-decadal catalogue from 1990 to 2024. This problem is not merely technical: if an interpolation method systematically underestimates magnitudes in certain areas, those locations may be undervalued in risk assessments, potentially leading to under-designed critical infrastructure or insufficient preparedness measures; conversely, overestimation may divert limited resources away from truly vulnerable communities. The question of “which method is more accurate” therefore translates directly into how confidently stakeholders can use interpolated magnitude maps to support disaster-risk-reduction decisions in Aceh’s high-consequence environment.

To address this problem, the present study pursues three specific objectives. First, it characterizes the spatial distribution of historical earthquake magnitudes ($M \geq 2.5$) in Aceh Province using a 34-year catalogue obtained from the USGS Earthquake Hazards Program, thereby providing a long-term view of seismicity patterns in the region [6]. Second, it implements IDW with a range of power parameters and Universal Kriging with several candidate semivariogram models to account for potential non-stationarity in the mean magnitude field, calibrating

each method using a leave-one-out cross-validation framework and standard error statistics. Third, it compares the predictive performance and resulting spatial patterns of IDW and Kriging, interpreting the differences considering Aceh's tectonic structure and discussing their practical implications for disaster risk reduction and spatial planning. In line with prior evidence that earthquake magnitudes and intensities often exhibit spatial autocorrelation along plate boundaries and fault systems, the working hypothesis is that Universal Kriging with an appropriately fitted semivariogram will outperform IDW, yielding lower cross-validated errors and more geologically coherent magnitude fields. IDW and Kriging are chosen as the focus of this study because they constitute transparent, widely adopted baselines in hazard mapping; more complex interpolation and machine-learning approaches are left for future work once the behavior of these foundational methods is fully understood in the Aceh context.

2. Materials and Methods

2.1. Study Area and Data Source

This study focuses on Aceh Province in the northern part of Sumatra, Indonesia, a region located along the Sunda megathrust and segmented strike-slip faults, which together generate frequent moderate to large earthquakes. The earthquake catalogue used in this analysis was obtained from the U.S. Geological Survey (USGS) Advanced National Seismic System (ANSS) Comprehensive Earthquake Catalog (ComCat) and Earthquake Hazards Program web service (https://earthquake.usgs.gov). The catalogue includes events with moment magnitude (Mw) ≥ 2.5 that occurred between 1 January 1990 and 31 December 2024 within a spatial window encompassing Aceh and its surrounding offshore areas (approximately 2–7° N and 94–99° E) [6].

From the downloaded catalogue, we retained the origin time, epicentral coordinates (latitude, longitude), focal depth, and magnitude. Events flagged as quarry blasts or other non-tectonic sources were excluded using the catalog's event type field. The remaining seismic events were then spatially filtered using the administrative boundary polygon of Aceh Province. Only events whose epicenters fell inside this polygon were used in the interpolation, ensuring that the resulting maps represent the seismicity within Aceh's jurisdictional extent.

2.2. Data Preprocessing

All spatial operations were conducted in a geographic information system (GIS) environment. Earthquake epicenters were initially provided in geographic coordinates (latitude/longitude, WGS 84). For distance calculations and semivariogram analysis, coordinates were projected to an appropriate Universal Transverse Mercator (UTM) zone covering northern Sumatra to minimize distortions in distance and area; this projected coordinate system was used for all geostatistical computations, while final maps were visualized back in WGS 84.

Basic quality control included checking for duplicated event IDs, missing magnitudes, and implausible coordinates; such records were removed. Descriptive statistics and boxplots of magnitude were used to identify statistical outliers. A small number of very high-magnitude events (e.g., Mw ≥ 7.5), which appear as outliers relative to the bulk of the catalogue, correspond to physically meaningful megathrust earthquakes that are critical for seismic hazard. Consequently, these extreme events were retained rather than removed, following the recommendation that geostatistical analyses in hazard contexts should preserve the full range of observed values [19–21].

To evaluate potential non-stationarity in the mean magnitude field, we inspected scatterplots of magnitude versus latitude and longitude and fitted locally weighted regression (LOESS) smoothers. These exploratory plots indicated a systematic variation in mean magnitude along both the trench-perpendicular and trench-parallel directions, suggesting that the assumption of a constant mean required by Ordinary Kriging may be violated. This motivated the use of Universal Kriging with an explicit trend component [22, 23].

2.3. Spatial Interpolation Methods

2.3.1. Inverse Distance Weighting (IDW)

Inverse Distance Weighting (IDW) is a deterministic interpolation method that estimates the value of a variable at an unsampled location s_0 as a weighted average of nearby observed values $Z(s_i)$ [24]. The IDW estimator can be written as shown in Equation 1:

$$\hat{Z}(s_0) = \sum_{i=1}^{n} w_i Z(s_i) \text{, with } w_i = \frac{d(s_0, s_i)^{-p}}{\sum_{j=1}^{n} d(s_0, s_j)^{-p}}, \quad (1)$$

where $\hat{Z}(s_0)$is the estimated earthquake magnitude at location s_0, $Z(s_i)$ is the observed magnitude at sample point s_i, $d(s_0, s_i)$ is the Euclidean distance between s_0 and s_i in the projected coordinate system, $p$is the power parameter controlling the rate at which influence decays with distance, and $n$is the number of neighboring points used for interpolation.

In this study, we implemented IDW using a variable search radius that always included the nearest five

observations. This choice reflects a compromise between capturing local detail and maintaining numerical stability: too few neighbors can create noisy "bull's-eye" patterns around individual epicenters, whereas too many neighbors can oversmooth spatial variation that is important for hazard interpretation [24]. Limited sensitivity checks with larger neighborhoods (8–10 points) produced qualitatively similar patterns and only marginal changes in error statistics; therefore, five neighbors were adopted as the standard setting. The power parameter p was varied between 1 and 5 in integer increments, and the optimal value was selected based on cross-validation performance.

2.3.2. Universal Kriging

Kriging is a geostatistical interpolation technique that models spatial autocorrelation via the semivariogram and produces best linear unbiased predictions under specified assumptions [24]. Because exploratory analysis suggested a non-constant mean magnitude across Aceh, we employed Universal Kriging (UK), which allows the mean to vary deterministically as a function of spatial coordinates, rather than Ordinary Kriging, which assumes a constant mean over the domain.

In Universal Kriging, the magnitude at location s is decomposed as shown in Equation 2:

$$Z(s) = m(s) + \varepsilon(s), \tag{2}$$

where $m(s)$is a deterministic trend function and $\varepsilon(s)$ is a zero-mean, second-order stationary random field. Here, $m(s)$ was modeled as a first-order polynomial in projected coordinates as shown in Equation 3:

$$m(s) = \beta_0 + \beta_1 x + \beta_2 y, \tag{3}$$

with $x$and $y$denoting easting and northing, respectively, and $\beta_k$regression coefficients estimated from the data. Residuals $\hat{\varepsilon}(s_i) = Z(s_i) - \hat{m}(s_i)$ were then used to compute an experimental semivariogram (Equation 4):

$$\gamma(h) = \frac{1}{2N(h)} \sum_{i=1}^{N(h)} [\hat{\varepsilon}(s_i) - \hat{\varepsilon}(s_i + h)]^2, \tag{4}$$

where $\gamma(h)$ is the semivariogram value at separation distance h, $N(h)$ is the number of data pairs separated by distance h, and $\hat{\varepsilon}(s_i)$ and $\hat{\varepsilon}(s_i + h)$ are residuals at locations separated by h.

Three standard semivariogram models spherical, exponential, and Gaussian were fitted to the experimental semivariogram by weighted least squares. These models are widely used in environmental and geoscientific applications and are recommended as flexible defaults when prior information about the correlation structure is limited [24]. Each model is characterized by a nugget, sill, and range parameter, which respectively represent microscale variability or measurement error, the total variance explained by spatial structure, and the distance beyond which values become effectively uncorrelated.

The Universal Kriging predictor at an unsampled location s_0 can be expressed as shown in Equation 5:

$$\hat{Z}(s_0) = \hat{m}(s_0) + \sum_{i=1}^{n} \lambda_i \hat{\varepsilon}(s_i), \tag{5}$$

where $\hat{m}(s_0)$ is the trend evaluated at s_0, λ_i are Kriging weights obtained by solving the Kriging system defined by the fitted semivariogram model, and n is the number of neighboring points used in the local neighborhood. To keep the neighborhood definition comparable with IDW, we again used the nearest five observations within a variable search radius for Kriging.

Ordinary Kriging was initially tested as a candidate model. However, residual diagnostics revealed spatial patterns in the Ordinary Kriging residuals and a semivariogram shape consistent with an unmodeled large-scale trend, supporting the use of Universal Kriging in which the trend is explicitly modeled and only residual spatial correlation is handled by the semivariogram [25].

2.4. Implementation

All data preprocessing and mapping were conducted using ArcGIS Pro and QGIS, while geostatistical computations (semivariogram estimation, model fitting, and Kriging) were performed in R with the "gstat" and "sp" packages. IDW interpolation used the standard implementation in the GIS software with the parameter settings described above. For Kriging, experimental semivariograms were computed using lag distances chosen to ensure a sufficient number of pairs per bin while covering approximately half of the maximum inter-point distance, following common geostatistical practice [25]. Semivariogram models were then fitted and checked by visual comparison and by examining the fit to experimental points, as well as by cross-validation error statistics.

2.5. Model Validation and Performance Metrics

To evaluate and compare the predictive performance of IDW and Universal Kriging, we applied leave-one-out cross-validation (LOOCV), which is widely used in comparative studies of spatial interpolation methods [24]. For each event in turn, the observation at location s_i was temporarily removed from the dataset, the interpolation model was refitted using the remaining $n - 1$ observations, and the value at s_i was predicted.

Repeating this procedure for all n events yielded a set of cross-validated predictions $\hat{y}_i$ corresponding to observed magnitudes y_i. The same LOOCV framework and neighborhood settings were used for both IDW and Kriging to ensure a fair comparison.

Predictive accuracy was quantified using several measures. The mean squared error (MSE) and root mean squared error (RMSE) are defined as shown in Equations 6 and 7, respectively:

$$MSE = \frac{1}{n}\sum_{i=1}^{n}(y_i - \hat{y}_i)^2, \quad (6)$$

$$RMSE = \sqrt{MSE}, \quad (7)$$

where n is the number of observations, y_i is the observed magnitude at location i, and $\hat{y}_i$ is the corresponding predicted magnitude. The mean error (ME) expressed as shown in Equation 8 was used as a measure of bias, with values close to zero indicating approximately unbiased predictions.

$$ME = \frac{1}{n}\sum_{i=1}^{n}(y_i - \hat{y}_i), \quad (8)$$

To express typical errors relative to the observed magnitude, we computed the mean absolute percentage error (MAPE), as shown in Equation 9:

$$MAPE = \frac{100}{n}\sum_{i=1}^{n}\left|\frac{y_i - \hat{y}_i}{y_i}\right|, \quad (9)$$

These metrics are commonly recommended in reviews of spatial interpolation performance because they capture complementary aspects of model behavior, overall error magnitude, systematic bias, relative error, and association strength [26].

For the semivariogram model selection within Kriging, the exponential, spherical, and Gaussian models were each evaluated using LOOCV. The primary criterion for selecting the "best" semivariogram model was the lowest RMSE. When RMSE differences were negligible, preference was given to the m odel with smaller absolute bias (ME) and better visual agreement between the modeled and experimental semivariograms. The final comparison between IDW and Universal Kriging was based on their LOOCV RMSE, MAPE, and ME.

3. Results and Discussion

3.1. Descriptive Characteristics of the Earthquake Catalogue

The 1990–2024 USGS catalogue for Aceh contains 2,255 events with Mw ≥ 2.5 (Figure 1). Magnitudes range from 2.5 to 9.1, with a mean of approximately 4.5, a median around 4.3, and an interquartile range dominated by moderate earthquakes (M 3.5–5.0). A small number of very large events (M ≥ 7.5), including the 2004 megathrust earthquake, appear as statistical outliers in the boxplot of magnitudes (Figure 2). These events, although extreme, are physically meaningful and crucial for seismic hazard, so they were retained in all subsequent analyses rather than being truncated or transformed away.

Spatially, epicenters cluster along the offshore subduction interface west of Banda Aceh, around Simeulue and Aceh Singkil, and along segments of the Great Sumatran Fault that cut through the mainland. This pattern reveals clear anisotropy: seismicity is elongated parallel to major tectonic structures rather than being uniformly distributed across the province. These descriptive statistics are not only useful context but also directly inform the interpolation: the presence of clustered, fault-controlled seismicity with a long upper tail in magnitudes shapes both the semivariogram and the behavior of IDW and Kriging in subsequent steps.

3.2. Semivariogram Analysis and Model Selection

Exploratory semivariogram analysis of the Universal Kriging residuals indicates that earthquake magnitudes in Aceh exhibit clear spatial autocorrelation up to a finite range (Figure 3). The experimental semivariogram increases with separation distance *h* before approaching a sill, consistent with a stationary residual field after removal of the large-scale trend in magnitude. This pattern confirms that magnitudes at nearby locations tend to be more similar than those far apart, providing empirical justification for using Kriging rather than relying solely on distance-based weighting as in IDW

Three standard semivariogram models spherical, exponential, and Gaussian were fitted to the experimental semivariogram. Parameter estimates (nugget, sill, range) are summarized in Table 1. All three models capture the general shape of the empirical semivariogram, but the exponential model yields slightly lower cross-validation errors and better visual agreement near the origin and around the practical range (Figure 3). The nugget term remains relatively small compared to the sill, suggesting that microscale variability and measurement error are present but do not dominate the total variance in magnitudes. The fitted range parameter indicates that spatial correlation extends over distances comparable to the spacing between major fault segments and offshore trench-parallel structures, echoing the underlying tectonics of the region.

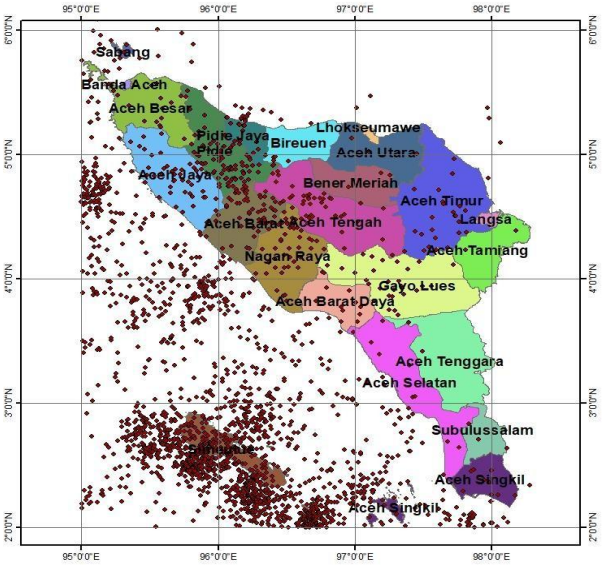

Figure 1. Map of earthquake epicenter locations in Aceh Province.

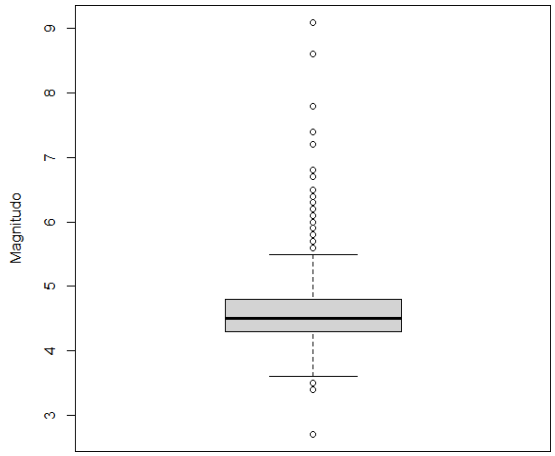

Figure 2. Boxplot of earthquake magnitudes showing outliers.

Table 1. Fitted semivariogram model parameters.

Model	Nugget	Sill	Range
Spherical	0.157	0.216	0.574
Exponential	0.157	0.216	0.574
Gaussian	0.157	0.216	0.574

3.3. Cross-validation Performance of IDW and Universal Kriging

Model performance was evaluated using leave-one-out cross-validation (LOOCV) for all IDW power parameters (p = 1–5) and for Universal Kriging with the three semivariogram models. Summary statistics of prediction accuracy RMSE, MSE, and MAPE are reported in Table 2.

For IDW, RMSE decreases modestly as the power parameter increases from p = 1 to p = 3, after which gains become negligible or even slightly reverse, consistent with the notion that excessively high powers overemphasize nearest neighbors and create noisy local surfaces. The best IDW configuration (here, p = 1) attains an RMSE of 0.2288 and a MAPE on the order of a few percent, with ME close to zero, indicating limited but non-negligible errors.

Universal Kriging with the exponential semivariogram outperforms all IDW settings, yielding a slightly lower RMSE (0. 0848), and marginally lower MAPE between observed and predicted magnitudes (Table 3). Although the numerical difference in RMSE between the best IDW and best Kriging models is modest, it is consistent and accompanied by reduced bias. Ordinary Kriging variants, by contrast, show slightly larger errors and stronger residual trends, supporting the choice of Universal Kriging in the presence of a non-constant mean magnitude field.

From a practical standpoint, an RMSE difference of approximately 0.005 in Mw may appear small, but it can be meaningful near critical magnitude thresholds used in engineering and risk communication, for example, distinguishing between moderate (M 5–6), strong (M 6–7), and major (M ≥ 7) events. A systematic under- or overestimation of even a few tenths of a magnitude unit can shift locations across such thresholds, altering how they are prioritized in seismic risk reduction strategies.

3.4. Spatial Patterns of Interpolated Magnitudes

Figures 4 and 5 present the spatial interpolation results for Aceh Province. IDW maps for different power values (Figure 4) show qualitatively similar large-scale patterns: higher predicted magnitudes are concentrated offshore along the Sunda megathrust, particularly west of Simeulue and Aceh Singkil, while lower magnitudes dominate inland areas with fewer moderate-to-large earthquakes. The colors in Figure 4 represent predicted magnitudes (Mw) at unsampled locations, derived from the 1990–2024 catalogue; warmer tones indicate higher expected magnitudes and cooler tones lower magnitudes.

As the power parameter p increases, the IDW surface becomes more locally influenced by nearest events. For p = 1, the surface is smooth and highlights broad gradients along the trench-parallel direction. For higher p (e.g., p = 4–5), the maps exhibit sharper local peaks around individual epicenters, producing "bull's-eye" artifacts in data-sparse regions. While such features may visually emphasize recent large earthquakes, they can be misleading for hazard interpretation because they exaggerate the influence of isolated events without considering the broader spatial correlation structure.

Universal Kriging with the exponential semivariogram yields a smoother yet geophysically coherent magnitude field (Figure 5). The map represents the expected

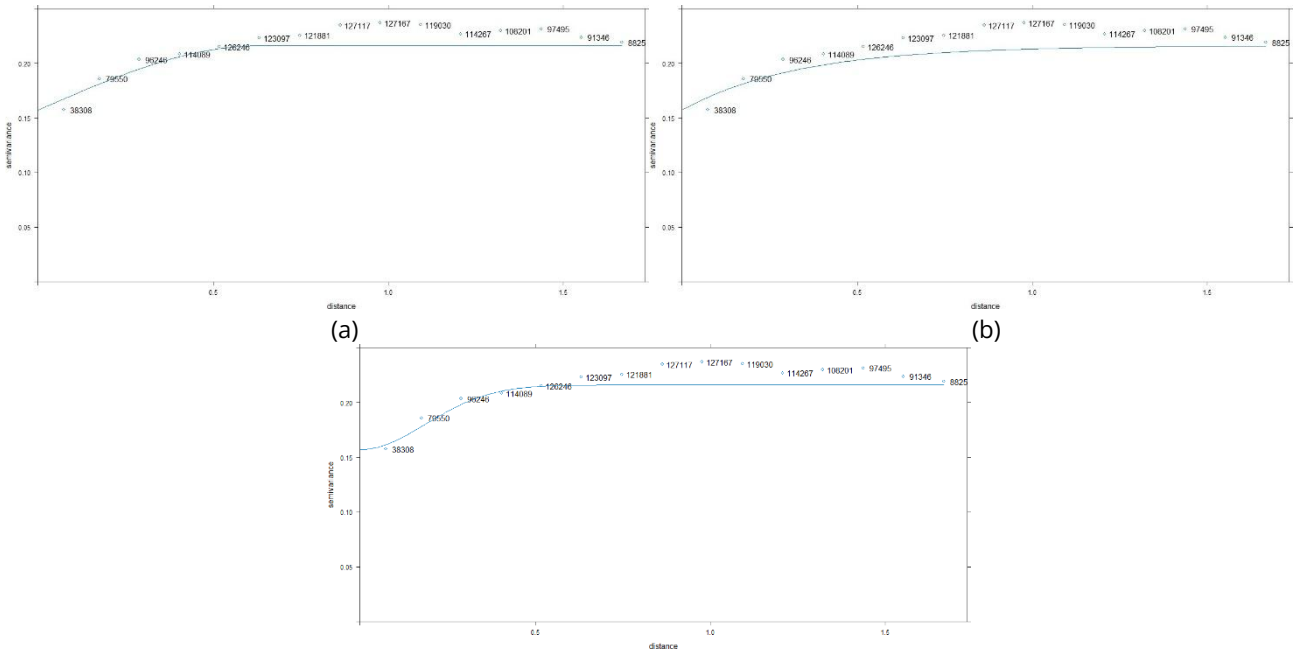

Figure 3. Experimental semivariogram and fitted models (a) spherical, (b) exponential and (c) Gaussian.

Table 2. Cross-validation accuracy of IDW interpolation under different power parameters

Power	RMSE	MSE	MAPE
1	**0.2288**	**0.0523**	**1.24**
2	0.2362	0.0558	1.28
3	0.2441	0.0596	1.32
4	0.2511	0.0630	1.35
5	0.2567	0.0659	1.38

Table 3. Cross-validation accuracy of theoretical semivariogram models.

Model	RMSE	MSE	MAPE
Spherical	0.1232	0.0151	2.24
Exponential	**0.0848**	**0.0072**	**1.14**
Gaussian	0.1094	0.0119	2.46

magnitude at each location given the historical catalogue and the estimated spatial autocorrelation not a deterministic forecast of specific future events. As in the IDW maps, higher expected magnitudes cluster along the offshore subduction interface and certain segments of the Great Sumatran Fault, aligning well with known tectonic structures. However, Kriging reduces the exaggerated local spikes produced by IDW and provides more gradual transitions between high- and low-magnitude zones, reflecting the underlying semivariogram structure.

The appearance of areas with predicted magnitudes ≥ 8 in some offshore segments under Kriging does not imply precise forecasts of future earthquakes of that exact size. Rather, these values should be interpreted as reflecting locations where historical large events and their spatial correlation lead to a high expected magnitude under the model. In other words, the interpolated surfaces describe a smoothed representation of the spatial pattern of past events over 1990–2024; they cannot by themselves predict the timing or exact size of future earthquakes, which depend on complex tectonic and temporal processes beyond the scope of purely spatial interpolation.

3.5. Outliers, Uncertainty, and Limitations

The influence of very large earthquakes such as the 2004 megathrust event is evident in both IDW and Kriging surfaces. Because these events were retained as outliers, they increase the local mean magnitude near their epicenters and contribute to elevated predicted magnitudes in surrounding offshore zones. In IDW, the impact of a single extreme event is largely controlled by the distance-based weighting and the choice of p, which can produce very high local peaks. In Kriging, the influence of such events is moderated by the semivariogram: while they still raise the local magnitude, the range and sill parameters limit how far their impact propagates and ensure that predictions remain consistent with the overall spatial correlation structure. This is one reason why Kriging yields smoother and arguably more realistic magnitude fields than IDW, particularly in data-sparse offshore regions.

Nevertheless, the interpolated maps should be interpreted with caution. First, the analysis focuses on mean predictions and does not explicitly map prediction variance or confidence intervals, so spatial uncertainty is

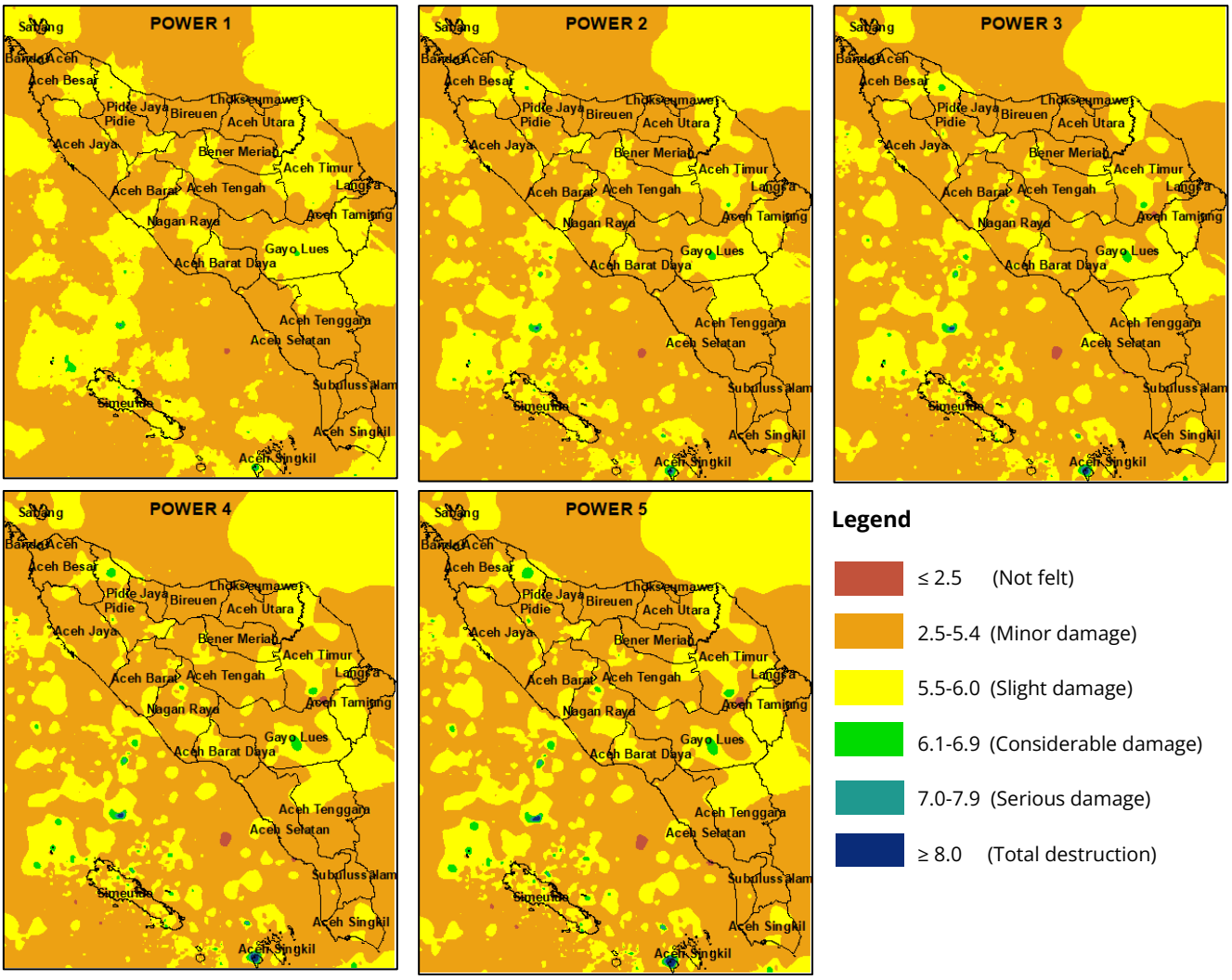

Figure 4. IDW interpolation maps at varying power parameters (1–5).

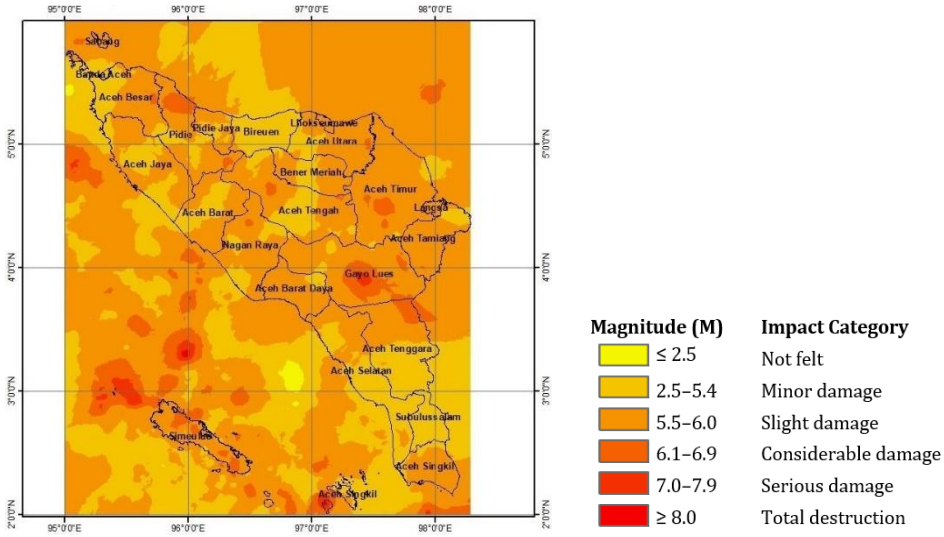

Figure 5. Spatial interpolation of earthquake intensity in Aceh Province using Kriging (Exponential Model).

not directly visualized. Predictions in areas with sparse data especially far offshore or in regions with few historical events are inherently less reliable than predictions in well-sampled zones. Kriging offers a formal way to quantify this via the Kriging variance, and future work should exploit this feature to produce accompanying uncertainty maps that identify where

additional monitoring or instrumentation would most improve hazard estimates.

Second, the interpolation is purely spatial and aggregates events over a 34-year period. It therefore provides a long-term view of where earthquakes have historically occurred, but it does not capture temporal clustering, changes in seismic regime, or evolving stress conditions. Changes in plate coupling, aftershock sequences, and slow-slip events can all modify future seismicity patterns relative to the historical record. Time-dependent seismic hazard models or point-process approaches would be required to address these aspects explicitly.

Third, while Universal Kriging with the exponential semivariogram appears to perform best among the tested methods, it is still based on relatively simple assumptions: a linear spatial trend and an isotropic semivariogram. The observed elongation of seismicity along faults suggests that anisotropic or direction-dependent variogram models could further improve realism. Likewise, more advanced approaches such as regression–Kriging with tectonic covariates, spatio-temporal models, or machine-learning methods may capture additional structure beyond what classical Kriging and IDW can represent. These extensions, however, are beyond the scope of the present benchmark comparison.

Despite these limitations, the results demonstrate that Kriging provides a modest but consistent improvement over IDW in representing the spatial pattern of historical earthquake magnitudes in Aceh, while also offering a framework to quantify uncertainty. For practice, the Kriging-based maps can serve as a long-term baseline for identifying zones where high-magnitude events have historically clustered and where attention to seismic design, retrofitting, and evacuation planning should be prioritized. Integrating these maps with exposure and vulnerability layers population, buildings, critical infrastructure would allow local authorities to convert the geostatistical outputs into actionable risk-reduction strategies.

4. Conclusions

This study set out to identify which of two widely used interpolation methods Inverse Distance Weighting (IDW) and Universal Kriging provides the most accurate and geophysically meaningful representation of the spatial distribution of earthquake magnitudes in Aceh Province, based on a 34-year USGS catalogue (1990–2024) of events with Mw ≥ 2.5. Using a consistent leave-one-out cross-validation framework and a common neighborhood definition, we found that Universal Kriging with an exponential semivariogram model systematically outperforms IDW across standard accuracy metrics. The best IDW configuration (p = 1) achieved an RMSE of 0.2288, whereas Universal Kriging reduced the RMSE to 0.0848 and yielded slightly lower MAPE, and smaller bias between observed and predicted magnitudes. Although the numerical differences are modest, they are consistent and indicate that explicitly modeling spatial autocorrelation provides measurable benefits over purely distance-based weighting.

The interpolated magnitude fields reveal coherent spatial patterns that align with Aceh's tectonic framework. Both IDW and Kriging highlight elevated expected magnitudes along the offshore Sunda megathrust and selected segments of the Great Sumatran Fault, with lower magnitudes dominating inland areas. However, IDW particularly at higher power parameters tends to produce "bull's-eye" artifacts and exaggerated local peaks around individual large events, especially in data-sparse regions. In contrast, Universal Kriging generates smoother and more geologically plausible gradients, because the semivariogram constrains how far and how strongly individual earthquakes influence surrounding locations. The resulting maps should therefore be interpreted as smoothed representations of the long-term spatial pattern of historical magnitudes rather than as deterministic forecasts of specific future events.

At the same time, several limitations and sources of uncertainty must be acknowledged. First, the analysis is purely spatial and aggregates events over a 34-year period; it does not capture temporal clustering, changes in seismic regime, or evolving stress conditions, so extrapolation to future seismicity requires caution. Second, only two interpolation families (IDW and Universal Kriging) were examined with relatively simple assumptions a linear spatial trend and an isotropic semivariogram despite clear evidence that seismicity is elongated along major faults. More complex methods, such as anisotropic variogram models, regression–Kriging with tectonic covariates, or spatio-temporal point-process models, may further improve realism but were beyond the scope of this benchmark comparison. Third, we focused on mean predictions and did not map the Kriging prediction variance, so users do not yet see where interpolated values are most uncertain; reliability is likely lower in offshore or inland regions with sparse historical data.

Despite these constraints, the findings have concrete implications for practice. The Kriging-based maps provide a transparent, data-driven baseline for identifying zones where high-magnitude events have historically clustered and where seismic-resistant design, retrofitting, and evacuation planning should be prioritized. In particular,

areas with interpolated magnitudes in the upper bands (e.g., Mw ≥ 6.5–7.0) can be treated as priority zones for stricter building codes, targeted community preparedness, and protection of critical infrastructure, provided that they are interpreted in conjunction with official national hazard maps. For future work, we recommend: (i) regularly updating the interpolation as new earthquake data become available; (ii) extending the analysis to include Kriging variance and uncertainty mapping; (iii) exploring anisotropic and regression-based geostatistical models that incorporate distance to faults, bathymetry, and site conditions; and (iv) testing hybrid frameworks that integrate geostatistics with machine-learning or physics-based seismic hazard models. Together, these steps would move from a static, spatially averaged picture of historical seismicity toward more comprehensive, probabilistic tools to support disaster risk reduction in Aceh.

Author Contributions: Conceptualization, L.R. and N.R.S.; methodology, N.R.S, and C.C.Y.U..; software, C.C.Y.U.; validation, R.F., and C.C.Y.U..; formal analysis, N.R.S and L.R.; investigation, L.R.; resources, C.C.Y.U.; data curation, N.R.S., and C.C.Y.U.; writing—original draft preparation, N.R.S., and R.F.; writing—review and editing, N.R.S., R.F., and L.R.; visualization, C.C.Y.U.; supervision, L.R.; project administration, L.R. All authors have read and agreed to the published version of the manuscript.

Funding: This study does not receive external funding.

Ethical Clearance: Not applicable.

Informed Consent Statement: Not applicable.

Data Availability Statement: Data is available upon request to the authors.

Acknowledgments: Thanks to the United States Geological Survey (USGS) for providing free access to data and making valuable contributions in support of this research

Conflicts of Interest: All the authors declare no conflicts of interest.

References

1. Rizal, J., Yodi Gunawan, A., W. Indratno, S., and Meilano, I. (2023). Seismic Activity Analysis of Five Major Earthquake Source Segments in the Sumatra Megathrust Zone, *Bulletin of the New Zealand Society for Earthquake Engineering*, Vol. 56, No. 2, 55–70. doi:10.5459/bnzsee.1555.
2. U.S. Geological Survey. (2004). M 9.1 - 2004 Sumatra - Andaman Islands Earthquake, *USGS Earthquake Hazards Program*.
3. Bilham, R. (2005). A Flying Start, Then a Slow Slip, *Science*, Vol. 308, No. 5725, 1126–1127. doi:10.1126/science.1113363.
4. Synolakis, C., Okal, E., and Bernard, E. (2005). The Megatsunami of December 26, 2004, *Bridge, National Academy of Engineering*, Vol. 32, No. 2, 25–35.
5. Alavi, S. H., Bahrami, A., Mashayekhi, M., and Zolfaghari, M. (2024). Optimizing Interpolation Methods and Point Distances for Accurate Earthquake Hazard Mapping, *Buildings*, Vol. 14, No. 6, 1823. doi:10.3390/buildings14061823.
6. U.S. Geological Survey. (n.d.). ANSS Comprehensive Earthquake Catalog (ComCat) and Earthquake Hazards Program: Catalog Documentation and Search Interface, *USGS Earthquake Hazards Program*.
7. Mase, L. Z. (2022). Local Seismic Hazard Map Based on the Response Spectra of Stiff and Very Dense Soils in Bengkulu City, Indonesia, *Geodesy and Geodynamics*, Vol. 13, No. 6, 573–584. doi:10.1016/j.geog.2022.05.003.
8. Swita, B., Astuti, M., Faisal, F., and Nuryaman, A. (2025). Mapping Earthquake Magnitudes In Bengkulu Province And Surrounding Areas Using Robust Ordinary Kriging, *BAREKENG: Jurnal Ilmu Matematika Dan Terapan*, Vol. 19, No. 3, 1537–1552. doi:10.30598/barekengvol19iss3pp1537-1552.
9. Hutchings, S. J., and Mooney, W. D. (2021). The Seismicity of Indonesia and Tectonic Implications, *Geochemistry, Geophysics, Geosystems*, Vol. 22, No. 9. doi:10.1029/2021GC009812.
10. Azhar, R., Rusdi, M., Irham, M., and Fuadi, A. (2021). Spatial Distribution of Mangrove Using a Geographic Information System in Aceh Besar, *IOP Conference Series: Earth and Environmental Science*, Vol. 674, No. 1, 012024. doi:10.1088/1755-1315/674/1/012024.
11. Nabila Azzahra Haris Putri, and Fauzan, A. (2024). Comparison of Inverse Distance Weighted and Thin Plate Spline Interpolation Methods in Projecting the Strength of the West Sumatra Earthquake, *EKSAKTA: Journal of Sciences and Data Analysis*, 185–193. doi:10.20885/EKSAKTA.vol5.iss2.art9.
12. AbdelRahman, M. A. E., Zakarya, Y. M., Metwaly, M. M., and Koubouris, G. (2020). Deciphering Soil Spatial Variability through Geostatistics and Interpolation Techniques, *Sustainability*, Vol. 13, No. 1, 194. doi:10.3390/su13010194.
13. Fatmawati, A. I., and Lubis, R. S. (2024). Estimated Sulfur Dioxide Pollutant Concentrations In Medan City Using Ordinary Kriging and Inverse Distance Weighting Approaches, *Mathline : Jurnal Matematika Dan Pendidikan Matematika*, Vol. 9, No. 1, 13–30. doi:10.31943/mathline.v9i1.548.
14. Wahid, M. A., and Winarno, E. (2024). Bauxite Resource Estimation Analysis Using Ordinary Kriging and Inverse Distance Weighting in West Kalimantan, *Journal of Earth and Marine Technology (JEMT)*, Vol. 4, No. 2, 255–264. doi:10.31284/j.jemt.2024.v4i2.5340.
15. Ananias, D. R. S., Liska, G. R., Beijo, L. A., Liska, G. J. R., and de Menezes, F. S. (2021). The Assessment of Annual Rainfall Field by Applying Different Interpolation Methods in the State of Rio Grande Do Sul, Brazil, *SN Applied Sciences*, Vol. 3, No. 7, 687. doi:10.1007/s42452-021-04679-1.
16. Guédé, K. G., Yu, Z., Hofmeister, F., Gu, H., Mohammadi, B., Chen, X., Lin, H., Shen, T., and Gouertoumbo, W. F. (2024). Geostatistical Interpolation Approach for Improving Flood Simulation Within a Data-Scarce Region in the Tibetan Plateau, *Hydrological Processes*, Vol. 38, No. 11. doi:10.1002/hyp.15336.
17. Aparecido, L. E. de O., Moraes, J. R. da S. C. de, Lima, R. F. de, and Torsoni, G. B. (2022). Spatial Interpolation Techniques to Map Rainfall in Southeast Brazil, *Revista Brasileira de Meteorologia*, Vol. 37, No. 1, 141–155. doi:10.1590/0102-77863710015.
18. Workneh, H. T., Chen, X., Ma, Y., Bayable, E., and Dash, A. (2024). Comparison of IDW, Kriging and Orographic Based Linear Interpolations of Rainfall in Six Rainfall Regimes of Ethiopia, *Journal of Hydrology: Regional Studies*, Vol. 52, 101696. doi:10.1016/j.ejrh.2024.101696.
19. Sawires, R., Santoyo, M. A., Peláez, J. A., and Corona Fernández, R. D. (2019). An Updated and Unified Earthquake Catalog from 1787 to 2018 for Seismic Hazard Assessment Studies in Mexico, *Scientific Data*, Vol. 6, No. 1, 241. doi:10.1038/s41597-019-0234-z.

20. Vorobieva, I. A., Gvishiani, A. D., Shebalin, P. N., Dzeboev, B. A., Dzeranov, B. V., Skorkina, A. A., Sergeeva, N. A., and Fomenko, N. A. (2023). Integrated Earthquake Catalog II: The Western Sector of the Russian Arctic, *Applied Sciences*, Vol. 13, No. 12, 7084. doi:10.3390/app13127084.

21. Maiti, S. K., and Kim, B. (2025). An Updated, Homogeneous, and Declustered Earthquake Catalog for South Korea and Neighboring Regions, *Natural Hazards and Earth System Sciences*, Vol. 25, No. 10, 4021–4041. doi:10.5194/nhess-25-4021-2025.

22. Pradhan, A., Adams, K. H., Chandrasekaran, V., Liu, Z., Reager, J. T., Stuart, A. M., and Turmon, M. J. (2024). Modeling Groundwater Levels in California's Central Valley by Hierarchical Gaussian Process and Neural Network Regression, *Journal of Geophysical Research: Machine Learning and Computation*, Vol. 1, No. 4. doi:10.1029/2024JH000322.

23. Healy, D., Tawn, J., Thorne, P., and Parnell, A. (2025). Inference for Extreme Spatial Temperature Events in a Changing Climate with Application to Ireland, *Journal of the Royal Statistical Society Series C: Applied Statistics*, Vol. 74, No. 2, 275–299. doi:10.1093/jrsssc/qlae047.

24. Li, J., and Heap, A. D. (2008). A Review of Spatial Interpolation Methods for Environmental Scientists, *Australian Geological Survey Organisation*, Vol. GeoCat# 68, No. 2008/23, 154. doi:http://www.ga.gov.au/image_cache/GA12526.pdf.

25. Webster, R., and Oliver, M. A. (2008). Geostatistics for Environmental Scientists: Second Edition, *Geostatistics for Environmental Scientists: Second Edition*, 1–315. doi:10.1002/9780470517277.

26. Li, J., and Heap, A. D. (2011). A Review of Comparative Studies of Spatial Interpolation Methods in Environmental Sciences: Performance and Impact Factors, *Ecological Informatics*, Vol. 6, Nos. 3–4, 228–241. doi:10.1016/j.ecoinf.2010.12.003.